JOURNAL OF SOLID STATE CHEMISTRY **133,** 587–590 (1997)
ARTICLE NO. SC977615

LETTER TO THE EDITOR

In situ Transmission X-Ray Absorption Fine Structure Analysis of the Charge–Discharge Process in $LiMn_2O_4$, a Rechargeable Lithium Battery Material

Youhei Shiraishi, Izumi Nakai,[1] Toshio Tsubata,* Takuhiro Himeda,* and Fumishige Nishikawa*

Department of Applied Chemistry, Faculty of Science, Science University of Tokyo, Kagurazaka, Shinjuku, Tokyo 162 Japan; and
**Battery Development Laboratory, Asahi Chemical Industry, Co., Ltd., Yako, Kawasaki, Kanagawa 210 Japan*

Communicated by J. M. Honig August 25, 1997; accepted September 8, 1997

The *in situ* XAFS technique has been applied for the first time to reveal variations in the local structures of Mn atoms during the charge–discharge process of $LiMn_2O_4$, $Li(Mn_{1.93}Li_{0.07})O_4$, and $Li(Mn_{1.85}Li_{0.15})O_4$ cathode materials of lithium-ion secondary batteries. It has been demonstrated that the valence state of manganese is in a linear correlation with the peak energy of the Mn *K*-edge XANES spectrum. EXAFS analysis disclosed the coexistence of Mn^{3+} and Mn^{4+} in $LiMn_2O_4$, with two distinct Mn–O bond distances of 1.98 and 1.88 Å for the Mn^{3+}–O_6 and Mn^{4+}–O_6 octahedra, respectively. Li deintercalation leads to the oxidation of Mn^{3+} to Mn^{4+} and finally to MnO_2, in which the Mn atom exhibits a uniform octahedral oxygen coordination, with a Mn–O distance of approximately. 1.9 Å The large variation in the local structure around the Mn atom during the charge–discharge process may be responsible for the cyclic instability of the battery material.

1. INTRODUCTION

Spinel manganese oxide, $LiMn_2O_4$, can be used industrially as the cathode material of lithium-ion rechargeable batteries, substituting for $LiCoO_2$, which is currently used in commercially available batteries (1–4). $LiMn_2O_4$ has advantages over $LiCoO_2$ and $LiNiO_2$ because of the low cost of manganese and other favorable environmental characteristics. However, it has disadvantages in its cyclic reversibility, showing a significant capacity loss with repeated charge–discharge cycles (5). Because of this problem, possible improvements in the cyclic reversibility of this material have been widely investigated. The mechanism for the capacity-loss process in the cathode material, however, has not yet been clarified.

A structural analysis of the cathode material will provide information useful for understanding this charge–discharge process. The powder X-ray diffraction technique has been widely applied for this purpose (6, 7), but this technique does not fully solve the problem because it only provides an average structure for the crystalline phases with long-range structural order. On the other hand, the X-ray absorption fine structure (XAFS) technique is suitable for obtaining information regarding the electronic and local structure of cathode materials without long-range order. Two regions of the XAFS spectrum are used in the present study. One is the X-ray absorption near edge structure (XANES), which provides information about the valence state and symmetry of the electron orbitals of the Mn atom. The other is the extended X-ray absorption fine structure (EXAFS), which produces information about bond length, coordination number, and the Debye–Waller factor of the coordination atoms for the Mn atom, such as O and Mn.

Ammundsen *et al.* first reported an XAFS analysis of stoichiometric $LiMn_2O_4$, $Li(Mn_{1.67}Li_{0.33})O_4$, and the acid- and base-treated materials in which the Li ion was deintercalated and reintercalated (8). They clarified that Li deintercalation by acid treatment of $LiMn_2O_4$ results in the oxidation of manganese, inducing a shortening of the Mn–O and Mn–Mn distances, whereas the manganese valence does not change as a result of the acid treatment of $Li(Mn_{1.67}Li_{0.33})O_4$. They concluded that Li is deintercalated during acid treatment of $LiMn_2O_4$, while it is ion-exchanged by H^+ in $Li(Mn_{1.67}Li_{0.33})O_4$.

We have recently developed a special cell for *in situ* XAFS measurements of lithium secondary batteries (9). This method allows us to obtain transmission XAFS data from cathode materials at any deintercalation–intercalation stage without disassembling the cell. The Li deintercalation behavior of $LiNiO_2$ and $LiCoO_2$ was clarified by this

[1] To whom correspondence should be addressed.

0022-4596/97 $25.00

technique (9). Since charge–discharge processes accompany redox reaction in transition metals that may suffer oxidation and moisture attack when exposed to air, it is important to obtain XAFS data without disassembling the cell. In the present study, the *in situ* technique is successfully applied for the first time to reveal variations in the electronic and local structure of the Mn atom during the charge–discharge process of lithium manganese oxides.

2. EXPERIMENTAL

Stoichiometric $LiMn_2O_4$ and lithium-excess $Li(Mn_{1.93}Li_{0.07})O_4$, $Li(Mn_{1.85}Li_{0.15})O_4$ were prepared by a sintering method from lithium carbonate and manganese dioxide. The compounds were assembled as cathodes of lithium batteries in *in situ* XAFS cells. The lithium metal was used as an anode, and, 1 M $LiBF_4$ in PC + EC was used as an electrolyte. The cells were subjected to the charge–discharge process for 50 min and then kept at rest for 30 min. The Mn *K*-edge XAFS spectra were measured in the transmission mode at various stages of the charge–discharge process. The measurements were carried out at BL-10B, Photon Factory (PF), KEK, Japan, using a Si(111) double-crystal monochromator. The XAFS spectra of rhodochrosite ($MnCO_3$), $MnPO_4$, and pyrolusite (MnO_2) were measured as references. The REX2 (10) and FEFF6.01 (11) computer programs were used for the analysis of the XAFS data. The electron back scattering factor and phase shift were calculated by FEFF 6.01.

3. RESULTS AND DISCUSSION

Figure 1 shows the Mn *K*-XANES spectra for the three lithium manganese oxides, $LiMn_2O_4$, $Li(Mn_{1.93}Li_{0.07})O_4$, and $Li(Mn_{1.85}Li_{0.15})O_4$. The XANES spectra of the reference materials for Mn^{2+} (rhodochrosite), Mn^{3+} ($MnPO_4$), and Mn^{4+} (pyrolusite) are also shown for comparison. The white-line peak of $LiMn_2O_4$ (point A in Fig. 1) is located at approximately 6.56 keV, and the inflection point (point B) of the edge region is at approximately 6.55 keV. These energies are close to those of the main peaks of pyrolusite (Mn^{4+}) and $MnPO_4$ (Mn^{3+}), respectively. Therefore, components A and B can be ascribed mainly to the Mn^{4+} and Mn^{3+} states, respectively. As is evident from Fig. 1, substitution of Li for Mn causes slight shifts of the edge to the higher energy side, due to an increase in the average valence of manganese. Figure 2 displays the Mn *K*-XANES spectra for $Li_xMn_2O_4$ as a function of x, measured during the charge–discharge process of the cell. The starting material was $LiMn_2O_4$ with stoichiometric composition. The value of x was calculated from the cathode active mass and the charge transfer. The Li ion was deintercalated first (charge process) to $Li_{0.09}Mn_2O_4$, which was then intercalated (discharge process) to $Li_{0.88}Mn_2O_4$. Because the amount of

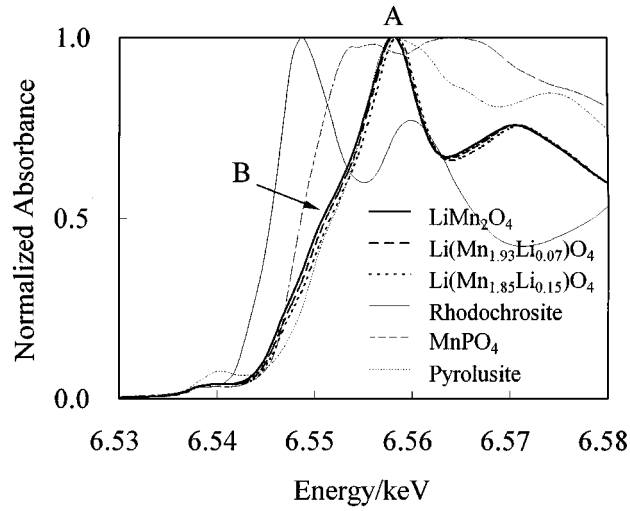

FIG. 1. Mn *K*-XANES spectra of lithium manganese oxides and several reference samples for several Mn valences. The highest absorbance of each spectrum was normalized to unity.

Mn does not change during the charge–discharge process, the XANES spectra were normalized at 7.62 keV, 1 keV above the absorption edge, where the absorption factor μ_{Mn} was expected to be constant, independent of structural variations. Electrochemical deintercalation of Li causes a continuous shift of the XANES spectra to the higher energy side, whereas the intercalation causes a backward shift of the spectra, indicating the reversibility of the reaction.

To consider the relationship between lithium content and the manganese valence, the energy of peak A was plotted in Fig. 3 against the Li content and the nominal manganese valence, which was calculated from the chemical formula

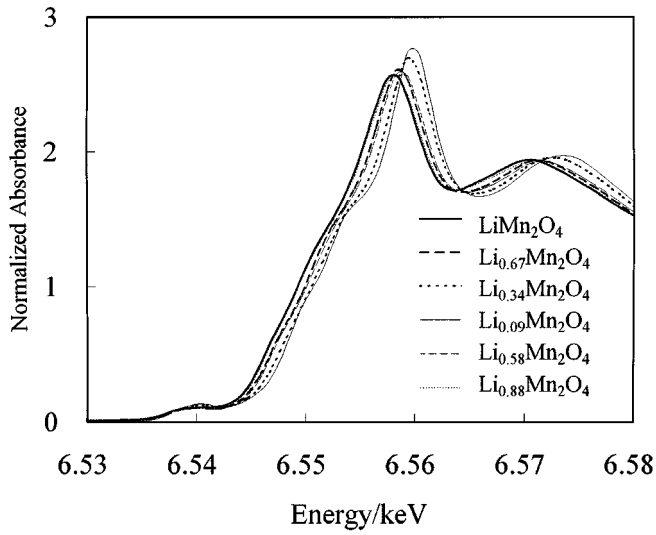

FIG. 2. Comparison of the Mn *K*-XANES spectra for $Li_xMn_2O_4$ as a function of x. The ordinate scales of the spectra were normalized at 7.62 keV (see text).

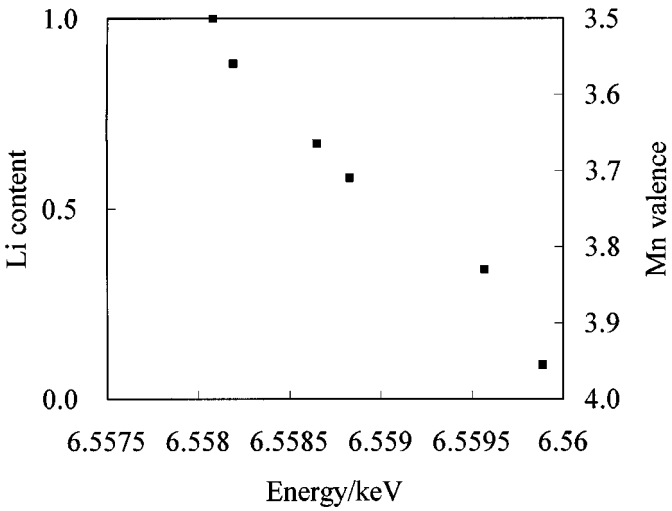

FIG. 3. Relationship between the energy of the white line in the Mn *K*-XANES spectra, the Li content, and the expected Mn valence for $Li_xMn_2O_4$.

TABLE 1
Structural Parameters of $Li_xMn_2O_4$ Obtained from the Curve-Fitting Analysis Assuming Octahedral Coordination of the Neighboring Atoms at Equal Distances[a]

Sample	Coordination atom	r/Å	σ/Å	R_f
$LiMn_2O_4$	O	1.921	0.087	7.31
	Mn	2.912	0.088	3.62
$Li_{0.67}Mn_2O_4$	O	1.918	0.086	4.86
	Mn	2.893	0.088	4.55
$Li_{0.34}Mn_2O_4$	O	1.913	0.078	4.81
	Mn	2.863	0.085	4.14
$Li_{0.09}Mn_2O_4$	O	1.917	0.076	4.79
	Mn	2.849	0.078	4.34
$Li_{0.58}Mn_2O_4$	O	1.916	0.083	6.88
	Mn	2.889	0.089	4.33
$Li_{0.88}Mn_2O_4$	O	1.911	0.090	6.60
	Mn	2.923	0.088	4.72

[a] Mean free path was fixed at 4.150 (coordination atom is oxygen) and at 4.235 (coordination atom is manganese), respectively.

$Li_xMn_2O_4$, based on electroneutrality. An almost linear relationship was found in this plot. This suggests that the manganese valence during the charge–discharge cycle of the cell could be estimated from the edge energy of the Mn *K*-XANES spectra.

Fourier transforms (FT) of the $k^3\chi(k)$ oscillation of the Mn *K*-EXAFS spectra of $Li_xMn_2O_4$ are shown in Fig. 4. The abscissa is the distance, which is not corrected for the phase shift, between the Mn atom and the coordinated atoms; the ordinate is the Fourier transform magnitude. The first peak at around 1.5 Å in FT corresponds to the Mn–O interaction in the first coordination sphere, and the second one at around 2.5 Å is the Mn–Mn interaction in the second coordination sphere. At a further distance, the peak at around 4.5 Å represents the second Mn neighbor at the central Mn atom, and the peak at around 5.5 Å is derived from the multiscattering caused by the Mn at twice the distance of the nearest Mn atom.

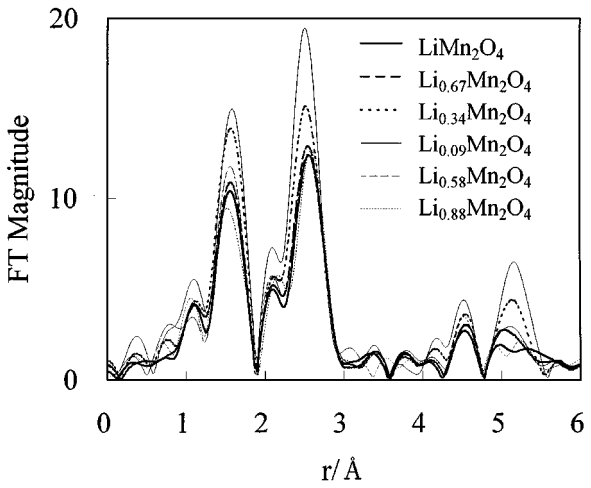

FIG. 4. Fourier transforms of EXAFS oscillation ($k^3\chi(k)$) for $Li_xMn_2O_4$ as a function of x.

Table 1 lists the structural parameters obtained from the curve-fitting analysis of $Li_xMn_2O_4$. The coordination atom of the first shell is oxygen, and that of the second shell is manganese. The mean free path of the photoelectron was fixed at 4.235 and 4.150 for the first and second shells, respectively, determined by the curve fitting analysis of $Li_{0.09}Mn_2O_4$, in which Mn was assumed to exhibit a regular MnO_6 octahedral coordination with an almost uniform valence of Mn^{4+}. In the spinel $LiMn_2O_4$ structure, the Mn atoms occupy the 16*d* site, which is coordinated by 6 O atoms at equal distance. The analysis, assuming octahedral coordination of the O atoms at equal distances, leads to the following result: the Mn–O distance does not vary with Li deintercalation, yielding a significantly large

TABLE 2
Structural Parameters of $LiMn_2O_4$ Obtained from the Curve-Fitting Analysis Assuming Various Mn–O Coordination Models[a]

Oxygen coordination	Coordination atom	r/Å	σ/Å	R_f
6	O	1.921	0.087	7.31
4 + 2	O1	1.906	0.045	2.19
	O2	1.996	0.020	
2 + 4	O1	1.882	0.015	2.82
	O2	1.968	0.045	
3 + 3	O1	1.893	0.032	2.10
	O2	1.983	0.032	

[a] Mean free path was fixed at 4.150.

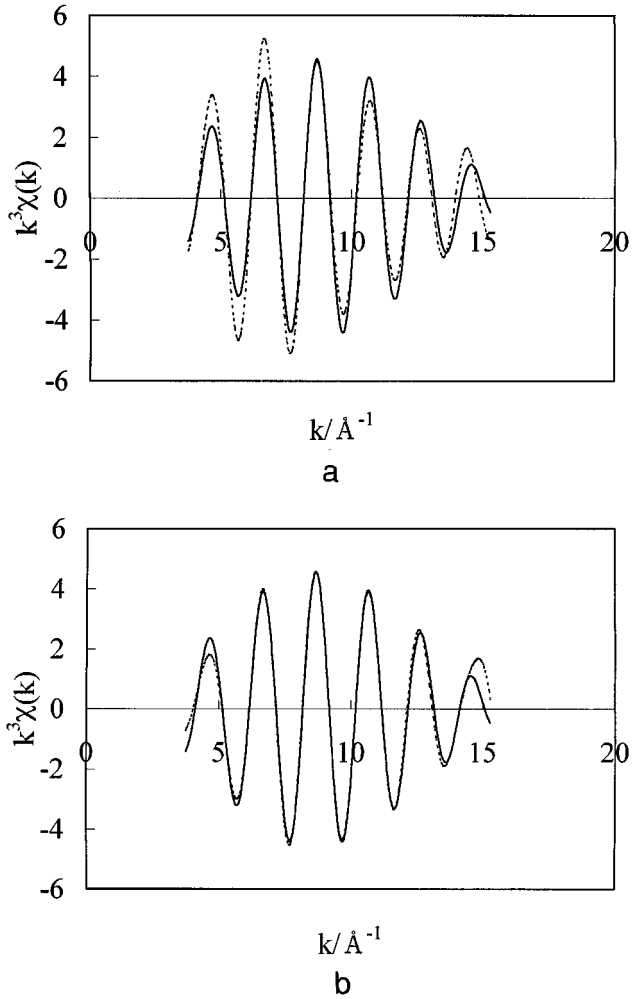

FIG. 5. Results of the curve-fitting analysis of $k^3\chi(k)$ EXAFS for $LiMn_2O_4$: (a) (3 + 3) Mn–O coordination model; (b) 6 equal Mn–O distance model.

residual factor (R_f) of 4.5–7.3 (Table 1). On the other hand, the Mn–Mn distance became shorter when Li was deintercalated, and became longer when it was intercalated.

All peaks in the FT increase in size when the cell is charged. A similar increase in amplitude, as well as a decrease in the Debye–Waller factor, determined for the Mn–O and Mn–Mn pairs, has been reported for the XAFS analysis of the Li^+ ion materials deintercalated–reintercalated by chemical treatment (8). They correlated this phenomenon with a decrease in the Debye–Waller factors, leading to the conclusion that the extraction of Li gave rise to local structure order. The peak height of the FT is related to the back scattering of the photoelectron by the coordinated atoms. However, when the coordinated atoms are not uniformly separated, the EXAFS oscillation tends to be counteracted. We assumed that the low peak height is due to the Mn ions existing as a mixed valence state of Mn^{3+} and Mn^{4+} in $LiMn_2O_4$, yielding two different local structures for Mn. On the other hand, in the fully charged state, Mn is oxidized to Mn^{4+}, yielding Mn_2O_4, in which Mn is expected to exhibit a uniform local structure. Moreover, Mn^{3+} is a d^4 Jahn–Teller ion; therefore, a distortion of the MnO_6 octahedra is also expected (2, 4). However, a curve-fitting analysis with a complex model such as the three different Mn–O distances did not yield physically meaningful results in the XAFS analysis. Therefore, we tried to analyze the EXAFS data based on the simplified (4 + 2), (3 + 3), and (2 + 4) coordination models for the different Mn–O bond distances in the Mn–O_6 octahedra. The (3 + 3) model gave the best results among the three models, with the lowest R_f and reasonable Debye–Waller factors (σ) listed in Table 2. The best fit $k^3\chi(k)$ for the (3 + 3) model is compared with that of the six equal Mn–O distance models in Figs. 5a and 5b, respectively.

Consequently, it is found that manganese in $LiMn_2O_4$ exhibits two distinct valences, Mn^{3+} and Mn^{4+}, with two kinds of MnO_6 octahedra, where the average Mn^{3+}–O and Mn^{4+}–O distances are 1.98 and 1.88 Å, respectively. The theoretical Mn–O distance calculated from the ionic radii (12) is 2.03 for Mn^{3+}–O (high spin state) and 1.91 Å for Mn^{4+}–O, in fair agreement with the present result. The electrochemical Li deintercalation causes the oxidation of Mn^{3+}, resulting in a uniform local structure for the Mn atom. This large-scale rearrangement of the local structure, accompanied by the charge–discharge process, may be responsible for the severe capacity-fading of $LiMn_2O_4$ with cycling when $LiMn_2O_4$ is used as a battery material.

ACKNOWLEDGMENTS

The XAFS experiments were performed with the approval of the PF Program Advisory Committee (#96G182).

REFERENCES

1. M. M. Thackeray, A. de Kock, and W. I. F. David, *Mater. Res. Bull.* **28,** 1041 (1993).
2. D. Guyomard and J. M. Tarascon, *Solid State Ionics* **69,** 222 (1994).
3. R. J. Gummow, A. de Kock, and M. M. Thackeray, *Solid State Ionics* **69,** 59 (1994).
4. J. M. Tarascon, W. R. McKinnon, F. Coowar, T. N. Bowmer, G. Amatucci, and D. Guyomard, *J. Electrochem. Soc.* **141,** 1421 (1994).
5. D. H. Jang, Y. J. Shin, and S. M. Oh, *J. Electrochem. Soc.* **143,** 2204 (1996).
6. V. Massarotti, D. Capsoni, M. Bini, C. B. Azzoni, and A. Paleari, *J. Solid State Chem.* **128,** 80 (1997).
7. M. N. Richard, I. Koetschau, and J. R. Dahn, *J. Electrochem. Soc.* **144,** 554 (1997).
8. B. Ammundsen, D. J. Jones, J. Roziere, and G. R. Burns, *Chem. Mater.*
9. I. Nakai, K. Takahashi, Y. Shiraishi, T. Nakagome, and F. Nishikawa, submitted for publication.
10. Rigaku, "EXAFS analysis software, REX2," Cat. No. 2612S211, Rigaku Co., 1996.
11. S. I. Zabinsky, J. J. Rehr, A. Ankudinov, R. C. Albers, and M. J. Eller, *Phys. Rev. B* **52,** 2995 (1995).
12. R. D. Shannon, *Acta Crystallogr. Sect. A* **32,** 751 (1976).